Available online at www.sciencedirect.com
SCIENCE DIRECT
International Journal of Heat and Mass Transfer 49 (2006) 1685–1695
International Journal of HEAT and MASS TRANSFER
www.elsevier.com/locate/ijhmt

Numerical simulation of fluid flow and convection heat transfer in sintered porous plate channels

Pei-Xue Jiang *, Xiao-Chen Lu

Key Laboratory for Thermal Science and Power Engineering, Department of Thermal Engineering, Tsinghua University, Beijing 100084, China

Received 24 February 2005; received in revised form 18 October 2005
Available online 27 December 2005

Abstract

Fluid flow and convective heat transfer of water in sintered bronze porous plate channels was investigated numerically. The numerical simulations assumed a simple cubic structure formed by uniformly sized particles with small contact areas and a finite-thickness wall subject to a constant heat flux at the surface which mirrors the experimental setup. The permeability and inertia coefficient were calculated numerically according to the modified Darcy's model. The numerical calculation results are in agreement with well-known correlation results. The calculated local heat transfer coefficients on the plate channel surface, which agreed well with the experimental data, increased with mass flow rate and decreased slightly along the axial direction. The convection heat transfer coefficients between the solid particles and the fluid and the volumetric heat transfer coefficients in the porous media predicted by the numerical results increase with mass flow rate and decrease with increasing particle diameter. The numerical results also illustrate the temperature difference between the solid particles and the fluid which indicates the local thermal non-equilibrium in porous media.

Keywords: Fluid flow; Convection heat transfer; Porous media; Permeability; Inertia coefficient; Temperature distributions

1. Introduction

Fluid flow and convection heat transfer in porous media have been widely investigated experimentally and numerically for many years due to the many important applications, such as catalytic and chemical particle beds, petroleum processing, geothermal energy extraction, transpiration cooling, packed-bed regenerators, solid matrix heat exchangers, micro-thrusters and many others. Porous media can intensify fluid mixing and increase the surface area in contact with the coolant, so porous structures are an effective heat transfer augmentation technique.

There have been numerous investigations with theoretical analyses and numerical simulations of convection heat transfer in fluid-saturated porous media. Vafai and Tien [1] investigated the nature and importance of the boundary and inertial effects on the flow and heat transfer in porous media. They showed that for the flow field, the boundary effects are confined to a very thin momentum boundary layer and often have no significant effect on the overall flow field. The effect of the boundary on the heat transfer, however, can be quite important. The inertial effects increase with permeability and decrease with fluid viscosity. The velocity gradients tend to increase near the wall, thereby increasing the viscous resistance at the boundary. The influence of the non-Darcian effects, variable porosity, variable properties and thermal dispersion in the porous medium on the fluid flow and heat transfer have been widely studied [2–7]. A comprehensive review of the heat and fluid flow characteristics in packed beds was published by Achenbach [8].

Numerical simulations of convection heat transfer in porous media are normally based on two different models for the energy equation, i.e. the local thermal equilibrium model and the local thermal non-equilibrium model. In recent years, the local thermal non-equilibrium model has

* Corresponding author. Tel.: +86 10 62772661; fax: +86 10 62770209.
E-mail address: jiangpx@tsinghua.edu.cn (P.-X. Jiang).

0017-9310/$ - see front matter © 2005 Elsevier Ltd. All rights reserved.
doi:10.1016/j.ijheatmasstransfer.2005.10.026

Nomenclature

a	Forchheimer parameter (1/m)
c_p	specific heat (J/kg K)
D_e	porous plate channel hydraulic diameter (m)
d_p	particle diameter (m)
F	inertia coefficient
h_{sf}	heat transfer coefficient between solid particles and fluid (W/m^2 K)
h_v	volumetric heat transfer coefficient (W/m^3 K)
h_x	local heat transfer coefficient (W/m^2 K)
H	enthalpy (J/kg)
K	porous medium permeability (m^2)
L	channel length (m)
Nu	Nusselt number
Δp	pressure drop (Pa)
q_{w0}	heat flux (W/m^2)
Re	Reynolds number based on the particle diameter ($=\varepsilon\rho u_p d_p/\mu$)
T	temperature (K)
u	fluid velocity (m/s)
U	velocity vector (m/s)
x, y, z	coordinates (m)

Greek symbols

ε	porosity
λ	thermal conductivity (W/m K)
μ	absolute viscosity (N s/m^2)
ρ	fluid density (kg/m^3)

Subscripts

0	inlet
b	bulk mean temperature
f	fluid
i	interface
s	solid particle
w	wall
x	local

been used more frequently in theoretical and numerical research of convection heat transfer in porous media [7,9–11] to more accurately model the convection heat transfer processes in porous media. With the thermal non-equilibrium model, the volumetric heat transfer coefficients between the solid particles and the fluid in the porous media and the treatment of the boundary conditions for the energy equation significantly affect the numerical simulation results. A number of papers have analyzed this problem [11–19]. Golombok et al. [20] employed the heat regenerator technique to measure the heat transfer coefficient between the flowing gas and the metal fibers of a burner. Their results showed that the heat transfer coefficient for laminar flow increased rapidly with increasing gas flow. Vafai and Sozen [21] analyzed the thermal-fluid characteristics for flow through a packed bed of spherical particles using fluid-to-solid heat transfer coefficients from an empirical correlation established by Gamson et al. [22]. Their results showed that the local thermal non-equilibrium condition was very sensitive to the particle Reynolds number and the Darcy number. Ichimiya [23] evaluated the convective heat transfer between the fluid and the solid material of aluminum–ceramic foam by comparing the measured and predicted Nusselt numbers on the heated wall of a porous channel. The constant heat flux boundary condition in porous media can be applied in several different ways. Alazmi and Vafai [11] analyzed eight different forms of constant wall heat flux boundary conditions in the local thermal non-equilibrium model. They found that different boundary conditions may lead to substantially different results, and selecting one model over the others is not an easy issue. In addition, the mechanics of splitting the heat flux between the two phases is not yet resolved.

Jiang et al. [17–19,24] experimentally and numerically investigated forced convection heat transfer of water and air in plate channels filled with non-sintered porous media (packed beds) or sintered porous media using a local thermal non-equilibrium model. They investigated the influences of boundary conditions on the convection heat transfer in porous media and the differences between the convection heat transfer in sintered and non-sintered porous media. Their results showed that for numerical simulations of convection heat transfer in porous media, the boundary condition model significantly influences the numerical results and the proper model must be chosen for the numerical simulation to agree well with the experimental data.

The present paper presents numerical simulations of the fluid flow and convection heat transfer in a simple cubic structure formed by uniform particles with small contact areas in a channel with a finite-thickness wall subject to a constant heat flux at the surface. The purpose of this study is to numerically determine the permeability, K, the inertia coefficient, F, the local heat transfer coefficient on the plate channel surface, h_x, the convection heat transfer coefficients between the solid particles and the fluid, h_{sf}, and the volumetric heat transfer coefficient, h_v, for convection heat transfer in porous media. The temperature distributions in the porous media are also analyzed. To the best of our knowledge, there is no other such analysis in the literature of the convection heat transfer in porous media. The direct numerical simulations of the fluid flow and convection heat transfer in porous media in the present paper establish a very good basis for further investigations of the boundary characteristics and internal phenomena controlling heat transfer in porous media.

2. Physical model, governing equations and numerical method

The sintered porous plate channel was made of bronze particles sintered to a thin copper plate placed in a stainless steel channel [24]. The upper copper plate of the test section was 1.0 mm thick. The sintered bronze material was a 89/11 copper/tin mix with a typical 0.3% phosphorous content. The nominal particle sizes of the sintered porous plates were 1.4–2, 1–1.4 and 0.5–0.71 mm. The hydraulic diameters of the sintered porous plate channels were 18.8, 19.9 and 21.4 mm. The porosities of the sintered porous plate channels were 0.463, 0.444 and 0.402.

A fully numerical solution of the Navier–Stokes equations for the fluid flow and convection heat transfer in a porous media with all the particles is very difficult due to the huge number of calculations. The present paper considers a limited number of identical particles as the porous media. The physical model and the coordinate system are shown in Fig. 1. The calculation region includes an entrance region with a length of $11d_p$ and an exit region with a length of $6d_p$. The packed beds consist of homogeneous, uniformly sized solid particles. Different porosities were obtained by changing the particle sizes and arrangements. The top surface of the porous media receives a constant heat flux, q_{w0}, while the bottom surface of the channel was thermally insulated. In the experimental research in Jiang et al. [24], the width of the porous plate channel was much larger than the channel height, and the side walls of the porous plate channel were thermally insulated. Therefore, to simplify the numerical calculations, the packed bed formed by the homogeneous, uniform solid particles was assumed to be periodic in the width direction. The fluid flow was assumed to be steady, single phase and three dimensional. Fluid enters the channel with a uniform velocity, u_0, and constant temperature, T_{f0}.

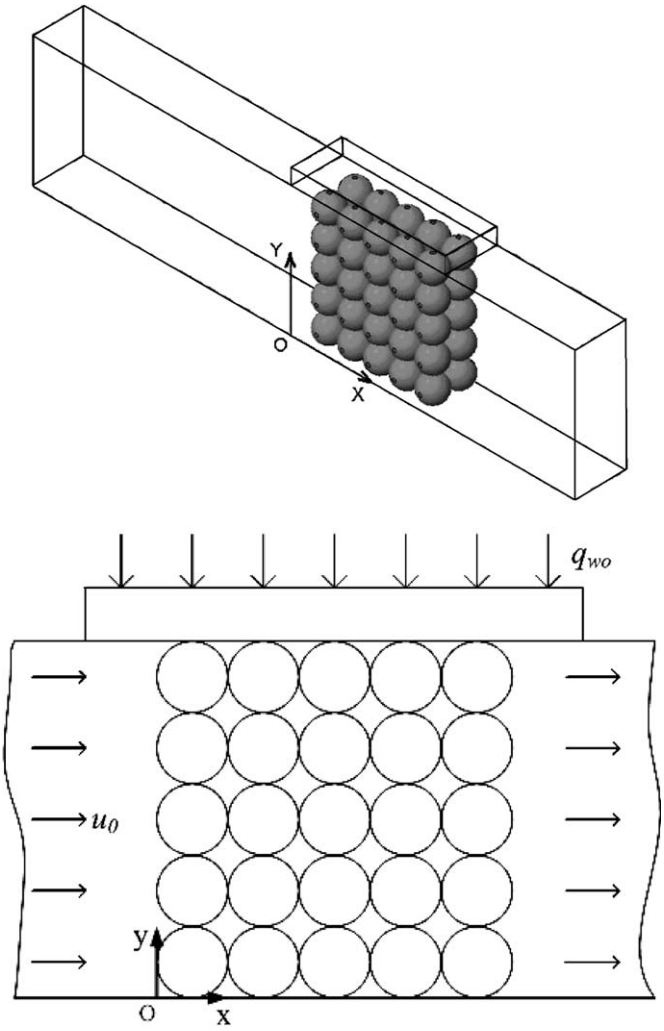

Fig. 1. Schematic diagram of the physical system.

Table 1 presents the dimensions and porosities of the porous media used in the calculations based on the experimental configuration in Jiang et al. [24]. The contact areas between the particles and the wall surface and the contact areas between particles were assumed to be constant based on the desired porosity. The other operating conditions in the numerical simulations were based on the experiments in Jiang et al. [24].

The numerical simulations used $5 \times 5 \times 2$ particles (length—x, height—y and width—z) with $d_p = 1.7$ mm, $5 \times 8 \times 1$ particles with $d_p = 1.2$ mm and $10 \times 18 \times 1$ particles with $d_p = 0.6$ mm. The numbers of particles in the y-direction were similar to the actual numbers of particles in the porous plate channels in the experiments [24]. The calculations assumed that the substrate wall was made of a copper plate of 1 mm thick. Water flows through the porous media and removes heat from the porous media and the impermeable wall. All the physical properties in the calculations were assumed to be constant.

The three-dimensional conjugate heat transfer problem was solved using the CFD software FLUENT 6.1. The Reynolds numbers based on the particle diameters and the inlet velocity were 4.57–231, thus, the fluid flow regimes in the porous media ranged from laminar, to transitional and to turbulent flow. The k–ω turbulence model was used in the numerical calculations for the turbulent flow. The SIMPLE algorithm was used to couple the pressure and velocities. The second-order upwind advection model was used in the momentum, turbulent kinetic energy, and turbulent energy dissipation equations.

The heat conduction equation for the upper copper plate of the test section is:

$$\nabla \cdot (\lambda_w \nabla T_w) = 0 \tag{1}$$

Table 1
Porous media dimensions and porosities

d_p (mm)	D_e (mm)		ε	
	Numerical	Experimental	Numerical	Experimental
1.7	16.8	18.8	0.458	0.463
1.2	18.9	19.9	0.450	0.444
0.6	20.5	21.4	0.396	0.402

The heat conduction equation for the solid particles is:

$$\nabla \cdot (\lambda_s \nabla T_s) = 0 \tag{2}$$

The mass, momentum and energy equations for the fluid are:

$$\nabla \cdot (\rho \mathbf{U}) = 0 \tag{3}$$

$$\nabla \cdot (\rho \mathbf{U}\mathbf{U}) = -\nabla p + \nabla \cdot \left(\mu\left(\nabla \mathbf{U} - \frac{2}{3}\nabla \cdot \mathbf{U}\boldsymbol{I}\right)\right) \tag{4}$$

$$\nabla \cdot (\rho \mathbf{U} H) = \nabla \cdot (\lambda_f \nabla T_f) \tag{5}$$

where $\boldsymbol{I}$ is the unit tensor.

The transport equations for k and ω are [25]:

$$\frac{\partial}{\partial x_i}(\rho k u_i) = \frac{\partial}{\partial x_j}\left(\left(\mu + \frac{\mu_t}{\sigma_k}\right)\frac{\partial k}{\partial x_j}\right) - \rho\overline{u_i' u_j'}\frac{\partial u_j}{\partial x_i} - \rho\beta^* f_{\beta^*} k\omega \tag{6}$$

$$\frac{\partial}{\partial x_i}(\rho \omega u_i) = \frac{\partial}{\partial x_j}\left(\left(\mu + \frac{\mu_t}{\sigma_\omega}\right)\frac{\partial k}{\partial x_j}\right) - \alpha\frac{\omega}{k}\rho\overline{u_i' u_j'}\frac{\partial u_j}{\partial x_i} - \rho\beta f_\beta \omega^2 \tag{7}$$

$$\mu_t = \alpha^* \frac{\rho k}{\omega}, \quad \alpha^*_\infty = 1, \quad \alpha_\infty = 0.52, \quad \alpha_0 = \frac{1}{9},$$
$$\beta^*_\infty = 0.09, \quad \beta_i = 0.072, \quad R_\beta = 8,$$
$$R_k = 6, \quad R_\omega = 2.95, \quad \varsigma^* = 1.5,$$
$$M_{t0} = 0.25, \quad \sigma_k = 2.0, \quad \sigma_\omega = 2.0$$

The conditions on the interface between the fluid and solid are:

$$T_f|_i = T_s|_i, \quad \lambda_f \nabla T_f|_i = \lambda_s \nabla T_s|_i \tag{8}$$

The unstructured mesh used 401,000–710,000 elements. Each particle had 400–800 nodes with 2000–4000 elements. The spaces between adjacent particles had about 500 nodes. Calculations with various numbers of elements showed that the results were grid independent. The convergence criteria required a decrease of at least 6 orders of magnitude for the residuals with no observable change in the surface temperatures for an additional 200 iterations.

3. Numerical results and discussion

3.1. Effective thermal conductivity of the porous media, λ_m

The reliability of the numerical analysis of the conjugate convection heat transfer and thermal conduction in porous media was verified by comparing the effective thermal conductivity of the porous media calculated from the numerical results with the values calculated from the equation proposed by Zehener [26]:

$$\frac{\lambda_m}{\lambda_f} = \left(1 - \sqrt{1-\varepsilon}\right) + \frac{2\sqrt{1-\varepsilon}}{1-\sigma B}\left[\frac{(1-\sigma)B}{(1-\sigma B)^2}\ln\left(\frac{1}{\sigma B}\right) - \frac{B+1}{2} - \frac{B-1}{1-\sigma B}\right]$$
$$B = 1.25[(1-\varepsilon)/\varepsilon]^{10/9}, \quad \sigma = \lambda_f/\lambda_s \tag{9}$$

The effective thermal conductivity of the porous media (Fig. 1) from the numerical results was calculated based on Fourier's law using the known heat flux on the top surface and the thickness of the porous media, with the numerically calculated temperature difference between the top and the bottom surfaces. The numerical model including the grid distributions was similar to that described above with the fluid velocity in the porous media set to zero.

For a porous medium with glass and water, the effective thermal conductivity predicted by Eq. (9) is $\lambda_m = 0.699$ W/(m K) for $\varepsilon_m = 0.354$. The numerical calculations predict 0.668 W/(m K) for the same porosity of $\varepsilon_m = 0.354$ which differs by 4.4%.

3.2. Permeability, K, and inertial coefficient, F

The momentum equation for low velocity, fully developed one-dimensional flow in a porous medium is represented by Darcy's law:

$$-\frac{dp}{dx} = \frac{\mu}{K}u \tag{10}$$

Forchheimer [27] pointed out that the departure of predictions by Darcy's law from measurements is due largely to the kinetic effect of the fluid which is not included in Darcy's low Reynolds number model. Therefore, Forchheimer suggested that a term representing the fluid kinetic energy, ρu^2, be included in Eq. (10), i.e.

$$-\frac{dp}{dx} = \frac{\mu}{K}u + a\rho u^2 \tag{11}$$

This additional term is often referred to as the Forchheimer term in the literature and, accordingly, the parameter a is called the Forchheimer constant. The most widely used expression for a is $F/(K)^{0.5}$. Although F is dimensionless, it is not a universal constant and is often found to vary with changes in porosity and structure of the porous medium. Eq. (11) can then be written as:

$$-\frac{dp}{dx} = \frac{\mu}{K}u + \frac{F}{\sqrt{K}}\rho u^2 \tag{12}$$

Kaviany [28] gave equations for K and F:

$$K = \frac{d_p^2 \cdot \varepsilon^3}{150(1-\varepsilon)^2} \tag{13}$$

$$F = \frac{1.75}{\sqrt{150}\varepsilon^{3/2}} \tag{14}$$

Eq. (12) can be rearranged in the form $Y = A + BX$ as:

$$-\frac{dp}{dx}\frac{1}{\mu u} = \frac{1}{K} + \frac{F}{\sqrt{K}}\frac{\rho u}{\mu} \tag{15}$$

The numerical results for the pressure drops at various velocities in the porous media were then fit with a least squares analysis to calculate K and F from the numerical results.

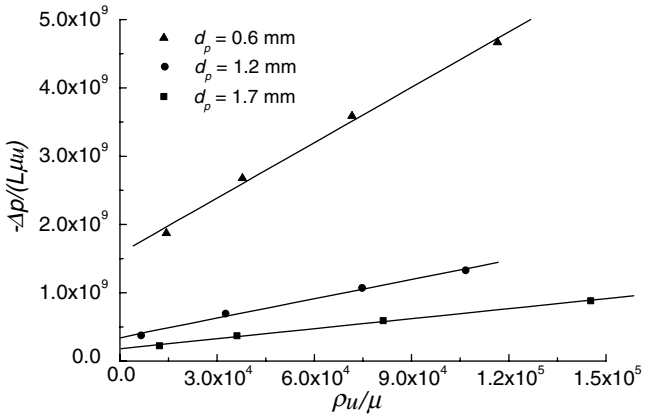

Fig. 2. Calculated flow resistances in the porous media for different velocities.

Table 2
Comparison between numerical and calculated results for K and F

d_p (mm)	1.7	1.2	0.6
ε	0.458	0.450	0.396
$1/K$ (m^{-2})	1.82×10^{8}	3.48×10^{8}	1.58×10^{9}
$F/(K)^{0.5}$ (m^{-1})	5230	9396	28963
K (m^2)	5.51×10^{-9}	2.87×10^{-9}	6.33×10^{-10}
F	0.388	0.503	0.729
K (m^2) (Eq. (13))	6.29×10^{-9}	2.89×10^{-9}	5.47×10^{-10}
F (Eq. (14))	0.461	0.473	0.519
Deviation of K	12.4%	0.7%	15.7%
Deviation of F	15.8%	6.34%	40.4%

Fig. 2 shows the three curve fits for the pressure drop for $d_p = 1.7$, 1.2 and 0.6 mm. The pressure drops were calculated using four different velocities for each particle size. The regression coefficients were all above 0.99. The intercepts and slopes increased with decreasing particle sizes. The permeability, K, and the inertia coefficient, F, were then calculated from the curve fits shown in Fig. 2.

Table 2 compares the values of K and F from the numerical results and those calculated using correlations (13) and (14) for the three particle diameters. The numerical results agree within 15% with the predictions of Eqs. (13) and (14) except for the relatively large deviation in F for the 0.6 mm diameter particles. The deviations between the numerical results and the correlations may be caused by the differences between the mean porosities in the numerical model and in the real porous plate channel and by the non-uniform particle diameters, non-uniform porosities and random particle distributions in the real porous media which differ from the ideal numerical model. The non-uniform particle diameters, non-uniform porosities and random particle distributions will be considered in future numerical simulations of the fluid flow and convection heat transfer in porous media.

3.3. Local heat transfer coefficient, h_x

The local heat transfer coefficient on the upper wall surface is defined as:

$$h_x = \frac{q_{w0}}{T_w(x) - T_{fb}(x)} \tag{16}$$

where $T_w(x)$ is the local wall temperature and $T_{fb}(x)$ is the local bulk fluid temperature.

Fig. 3 compares the calculated local heat transfer coefficients for convection heat transfer of water in the sintered bronze porous plate channels with the experimental data [24] for the 1.7, 1.2 and 0.6 mm diameter particles. Results were calculated using three different velocities for each

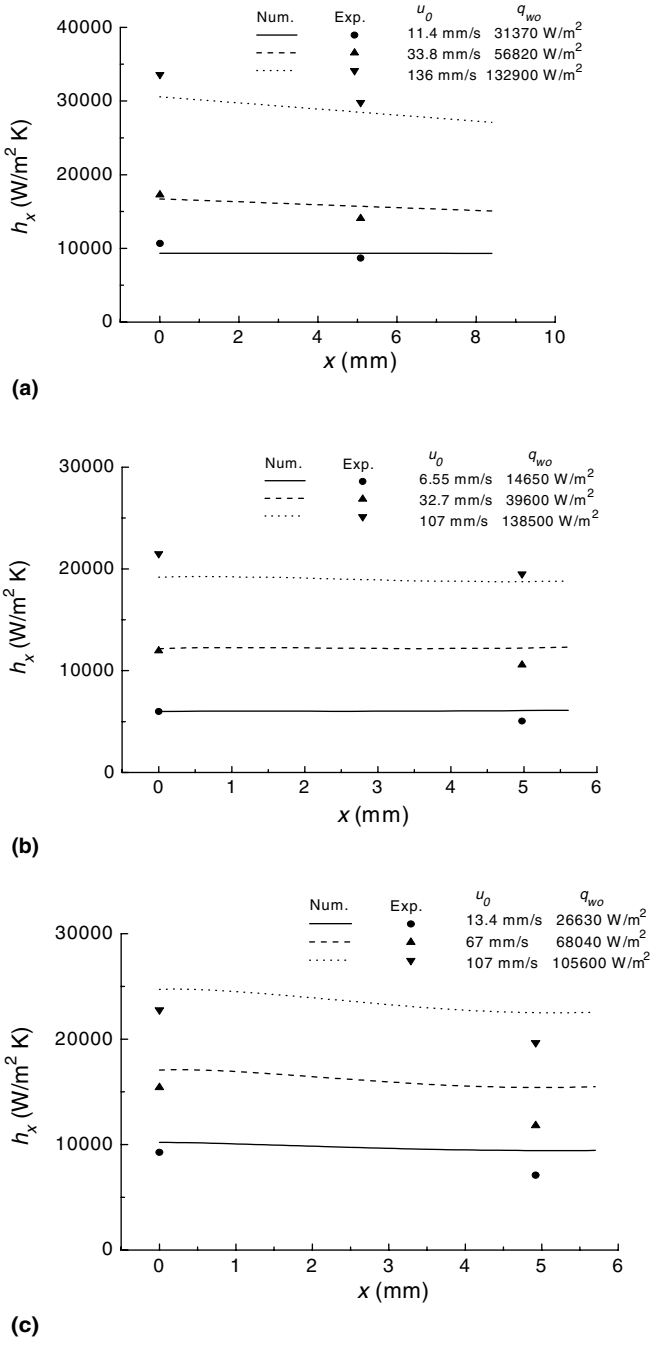

Fig. 3. Comparison of numerical results and experimental data for the local heat transfer coefficients for water in the sintered bronze porous channel. (a) $d_p = 1.7$ mm and $\varepsilon_m = 0.458$, (b) $d_p = 1.2$ mm and $\varepsilon_m = 0.450$, and (c) $d_p = 0.6$ mm and $\varepsilon_m = 0.396$.

particle size. The local heat transfer coefficients increased with mass flow rate (Reynolds number) and decreased slightly along the axial direction. The deviations between the calculated and experimental results were mostly less than ±20%. The deviations of the numerical results from the experimental data are probably also due to the differences between the mean porosities in the numerical model and in the real porous plate channel and the non-uniformity of the real porous media in the experiments. In general, the numerical results in Fig. 3 agree well with the experimental data, indicating that direct numerical simulations can model the fluid flow and heat transfer in the complete porous media. Future investigations will consider the effects of non-uniform particle diameters, non-uniform porosities and random particle distributions on the heat transfer in porous media.

3.4. Convection heat transfer coefficient between the solid particles and the fluid

The volumetric heat transfer coefficient between the solid particles and the fluid in the porous media, h_v, is an important parameter in the local thermal non-equilibrium model. There are several different experimental correlations for h_v, including the following proposed by Dixon and Cresswell [29]:

$$\frac{1}{h_{sf}} = \frac{d_p}{Nu_{sf}\lambda_f} + \frac{d_p}{\beta\lambda_s} \tag{17}$$

$$Nu_{sf} = \frac{0.255}{\varepsilon} Pr^{1/3} Re^{2/3}, \quad \beta = 10$$

and proposed by Wakao and Kaguei [30]:

$$h_{sf} = \left(2 + 1.1 Re^{0.6} Pr^{1/3}\right) \frac{\lambda_f}{d_p} \tag{18}$$

$$Re = \varepsilon \rho u_p d_p / \mu$$

In the present study, the detailed temperature distributions in the porous media were used to calculate the convection heat transfer coefficient between the solid particles and the fluid in the porous media as:

$$h_{sf} = \frac{q_{sf}}{T_s - T_f} \tag{19}$$

For each solid particle, T_s is calculated as the average temperature of the entire solid particle, T_f is the average fluid temperature in the cubic cell around the solid particle, and q_{sf} is the average heat flux through the solid particle's surface.

The volumetric heat transfer coefficient between the solid particles and the fluid, h_v, is defined as:

$$h_v = \frac{q_v}{T_s - T_f} \tag{20}$$

where q_v is the volumetric heat flux transferred from the solid to the fluid. h_v was calculated from the convection heat transfer coefficient between the solid particles and the fluid in the porous media, h_{sf}, using [8]:

$$h_v = h_{sf} \cdot 6(1-\varepsilon)/d_p \tag{21}$$

Fig. 4 compares the average temperatures of the solid particles in the second row of particles from the top with the average fluid temperature around the solid particles in the porous media for $d_p = 1.7$, 1.2 and 0.6 mm and different velocities. The results clearly illustrate the temperature difference between the solid particles and the fluid which indicates the importance of the thermal non-equilibrium model in the analysis of heat transfer in porous

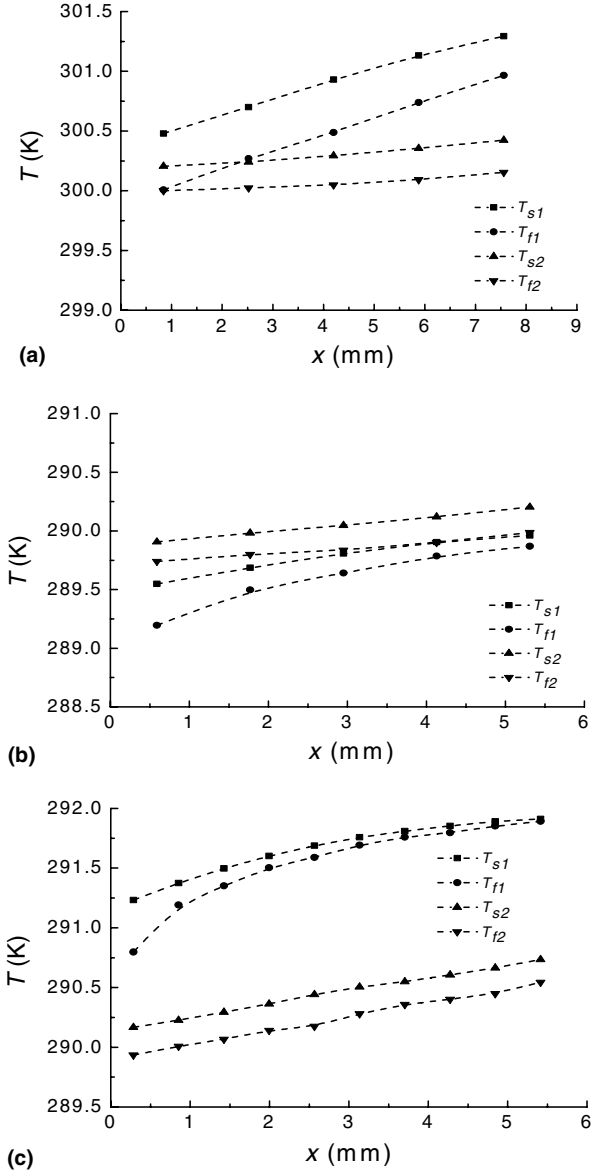

Fig. 4. Average temperatures of the second row of solid particles and the fluid around particles in the porous media. (a) $d_p = 1.7$ mm, $\varepsilon_m = 0.458$; 1—$u_0 = 11.4$ mm/s, $T_{f0} = 300.0$ K, $Re = 22.6$, $q_{w0} = 31{,}730$ W/m^2; 2—$u_0 = 136$ mm/s, $T_{f0} = 300.0$ K, $Re = 269.8$, $q_{w0} = 132{,}900$ W/m^2, (b) $d_p = 1.2$ mm, $\varepsilon_m = 0.450$; 1—$u_0 = 6.55$ mm/s, $T_{f0} = 289.17$ K, $Re = 7.1$, $q_{w0} = 14{,}650$ W/m^2; 2—$u_0 = 107$ mm/s, $T_{f0} = 289.74$ K, $Re = 117.5$, $q_{w0} = 138{,}500$ W/m^2, and (c) $d_p = 0.6$ mm, $\varepsilon_m = 0.396$; 1—$u_0 = 7.62$ mm/s, $T_{f0} = 290.66$ K, $Re = 4.3$, $q_{w0} = 19{,}810$ W/m^2; 2—$u_0 = 109$ mm/s, $T_{f0} = 289.93$ K, $Re = 60.1$, $q_{w0} = 105{,}600$ W/m^2.

media. For the lower fluid velocity, the temperature difference decreases along the flow direction, while the temperature difference changes little for the higher fluid velocity.

Fig. 5 presents the average heat flux distribution on the solid particle surfaces in the second row of particles from the top for $d_p = 1.7$, 1.2 and 0.6 mm. For the lower fluid velocity, the heat flux on the solid particle surfaces in the second row of particles decreases along the flow direction, while for the larger fluid velocity, the heat flux on the solid particle surfaces in the second row of particles increases at first, then decreases along the flow direction. This can be explained by the influence of the thermal boundary layer and thermal penetration effects. The temperature distribution in the solid particles and in the fluid in a plane passing through the centers of the particles is shown in Fig. 6. The figure shows that the thermal penetration thickness and the thermal boundary layer increase along the flow direction with an obvious temperature difference between the solid particles and the surrounding fluid. The thermal penetration and thermal boundary layer thicknesses both decrease with increasing flow velocity.

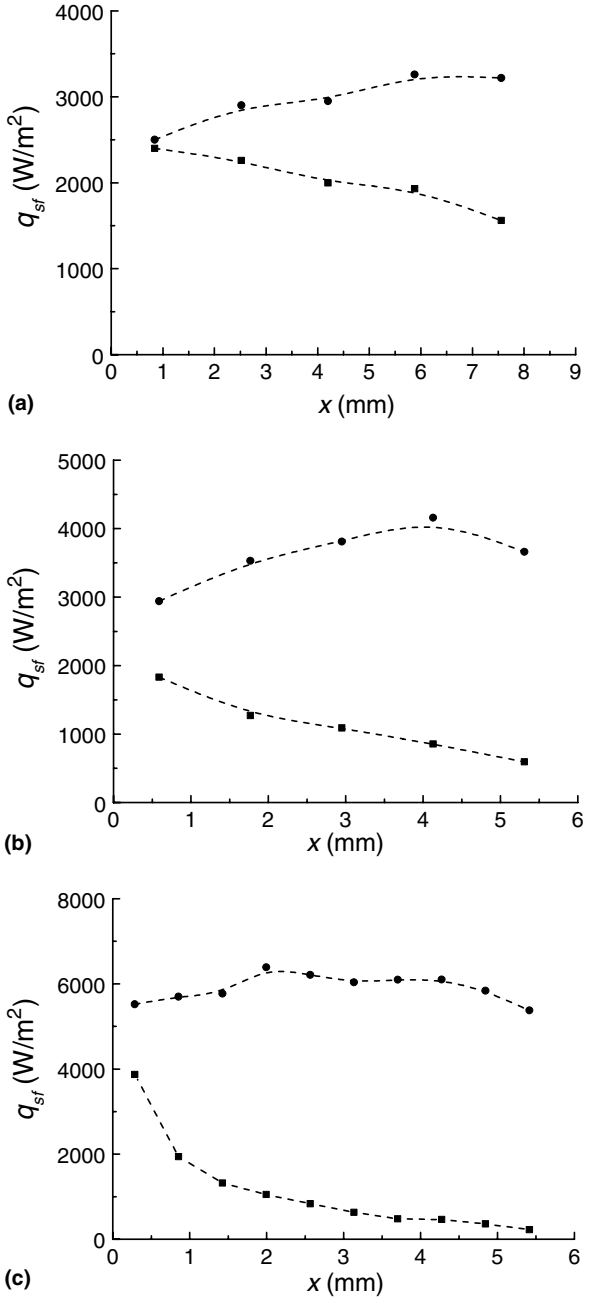

Fig. 5. Average heat flux distributions on the second row of solid particles. (a) $d_p = 1.7$ mm, $\varepsilon_m = 0.458$; (■)—$u_0 = 11.4$ mm/s, $T_{f0} = 300.0$ K, $Re = 22.6$, $q_{w0} = 31{,}730$ W/m^2; (●)—$u_0 = 136$ mm/s, $T_{f0} = 300.0$ K, $Re = 269.8$, $q_{w0} = 132{,}900$ W/m^2, (b) $d_p = 1.2$ mm, $\varepsilon_m = 0.450$; (■)—$u_0 = 6.55$ mm/s, $T_{f0} = 289.17$ K, $Re = 7.1$, $q_{w0} = 14{,}650$ W/m^2; (●)—$u_0 = 107$ mm/s, $T_{f0} = 289.74$ K, $Re = 117.5$, $q_{w0} = 138{,}500$ W/m^2, and (c) $d_p = 0.6$ mm, $\varepsilon_m = 0.396$; (■)—$u_0 = 7.62$ mm/s, $T_{f0} = 290.66$ K, $Re = 4.3$, $q_{w0} = 19{,}810$ W/m^2; (●)—$u_0 = 109$ mm/s, $T_{f0} = 289.93$ K, $Re = 60.1$, $q_{w0} = 105{,}600$ W/m^2.

For the lower fluid velocities with Reynolds numbers on the order of 10, the thermal boundary layer is relatively thick (as shown in Fig. 6), and the heat transferred from the top surface is conducted through the first row of solid particles to the second and following rows of particles from the top. At the same time, heat is transferred from the solid particles to the fluid by convection heat transfer. Fig. 6 shows that for the conditions studied here with the lower fluid velocities, the thermal penetration thickness is more than twice the particle diameter. Since the heat flux on the top surface is constant and the thermal boundary layer and the thermal penetration thicknesses increase along the flow direction, more and more heat is transferred from the solid particles in the third and following rows to the fluid along the flow direction. Therefore, the heat flux on the particle surfaces in the second row (from the top) decreases along the flow direction.

For the larger fluid velocities which have Reynolds numbers on the order of 100, the thermal boundary layer and the thermal penetration thickness in the first few columns is relatively small (less than twice the particle diameter as shown in Fig. 6); therefore, the convection heat transfer between the solid particles in the first row (from the top) to the fluid is very intense and there is little heat transfer from the solid particles in the first column of the second row to the flow. The thermal boundary layer and the thermal penetration thicknesses increase along the flow direction as more heat is conducted from the top surface through the solid particles in the second row to the flow, so that the heat transfer from the solid particles in the second row (from the top) to the fluid increases in subsequent columns. However, with further increases in the thermal boundary layer and thermal penetration thicknesses along the flow direction, more heat is conducted through the solid particles to the third and following rows and then to the fluid; therefore, the heat transfer from the solid particles in the second row to the fluid decreases further along the channel.

Fig. 7 presents the average heat flux distribution on the solid particle surfaces in the vertical direction for $d_p = 1.2$ mm and $\varepsilon_m = 0.450$. The results again clearly show the variations of the thermal penetration thickness and the

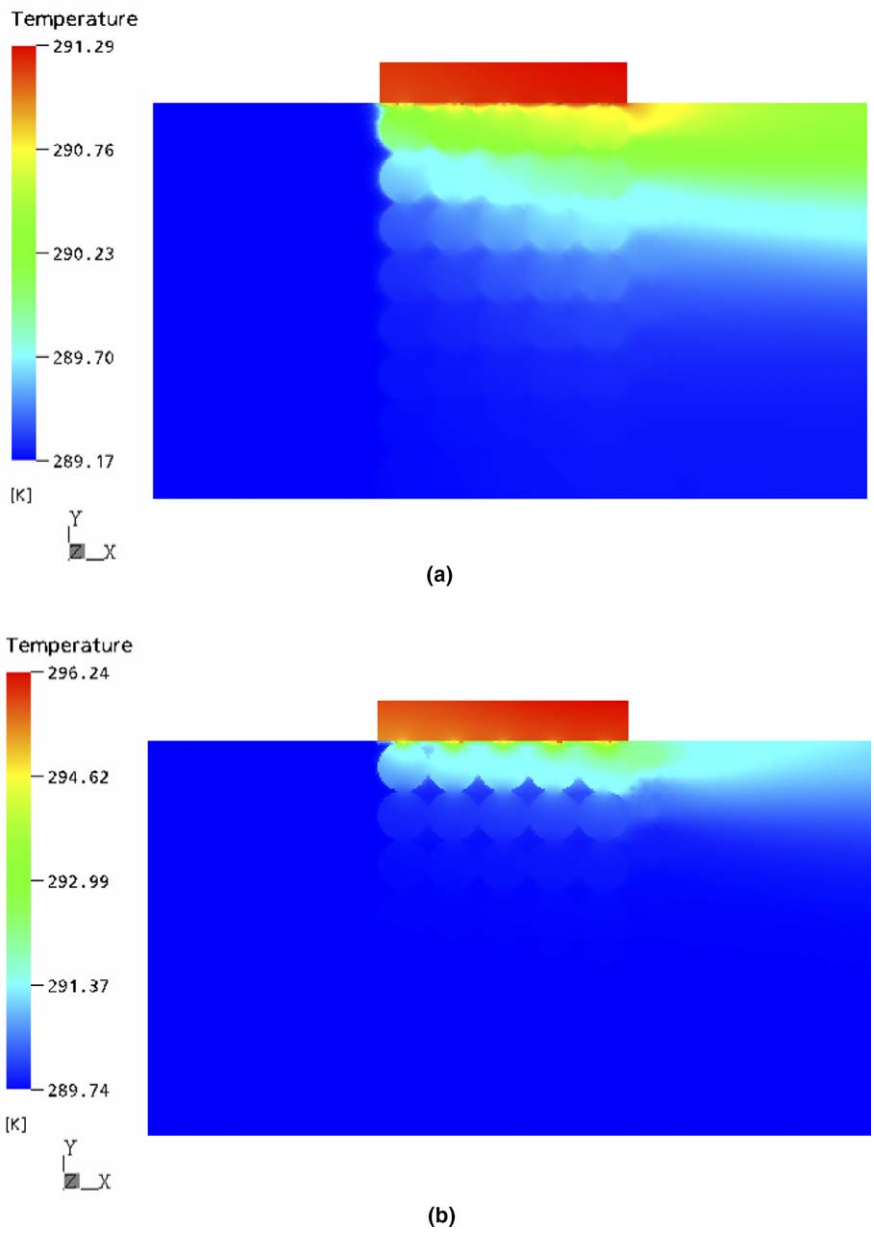

Fig. 6. Temperature field in the solid particles and in the fluid in a plane passing through the centers of the particles for $d_p = 1.2$ mm and $\varepsilon_m = 0.450$. (a) $Re = 7.1$, $T_{f0} = 289.17$ K, $q_{w0} = 14{,}650$ W/m^2 and (b) $Re = 117.5$, $T_{f0} = 289.74$ K, $q_{w0} = 138{,}500$ W/m^2.

average heat flux distribution on the solid particle surfaces for different conditions. Fig. 7(b) shows that the ratio of the average heat flux on the solid particle surfaces to the heat flux on the top surface decreases with increasing flow velocity due to the enhancement of the convection heat transfer on the top surface.

Fig. 8(a) shows the surface heat transfer coefficients between the fluid and the solid particles in the second row from the top for different particle diameters and fluid velocities. The heat transfer coefficients increase with fluid velocity and decrease with particle diameter. The heat transfer coefficient for a particle in the first column is approximately equal to that for a single particle in cross flow. The influence of the fluid flow and heat transfer from the particles in the front column on the heat transfer for the particles in the following columns is very weak due to the close contact between particles. Therefore, the heat transfer coefficients do not change much along the x-direction. For very high velocities and very large Reynolds numbers, the particles in the first few columns would act as a turbulence grid which would be expected to increase the heat transfer coefficient for particles in the following rows. In most configurations, however, the heat transfer conditions stabilize so that the particle convection coefficients are essentially constant beyond the fourth or fifth row [31]. Since porous media usually have many columns of solid particles, the heat transfer coefficient between the fluid and the solid particles can be assumed to not vary along the flow direction.

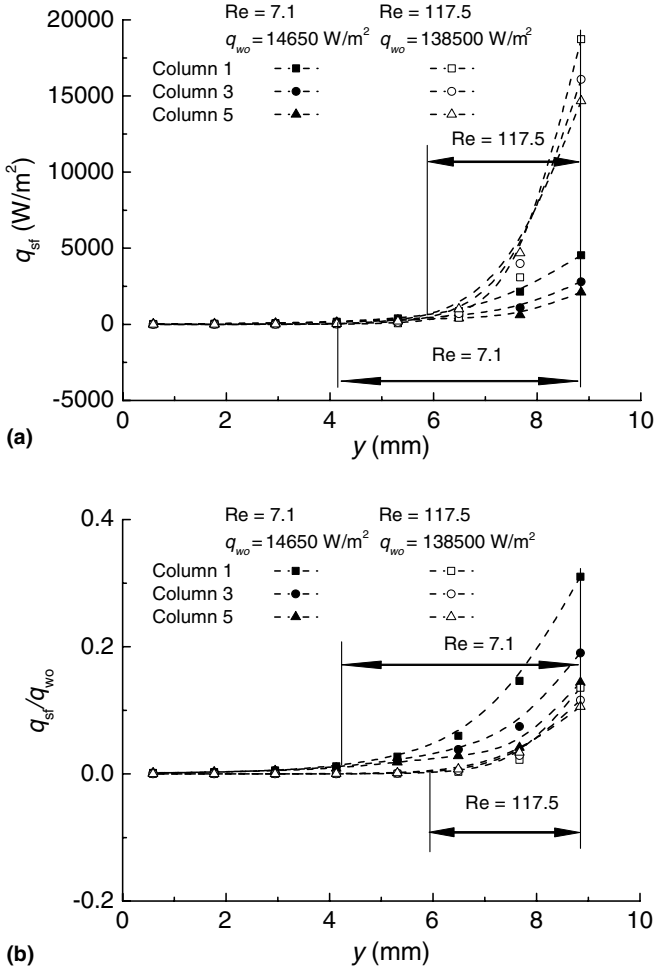

Fig. 7. (a) Average heat flux distribution in the vertical direction on the solid particle surfaces and (b) ratio of the average heat flux on the solid particle surfaces to the heat flux on the top surface for $d_p = 1.2$ mm and $\varepsilon_m = 0.450$.

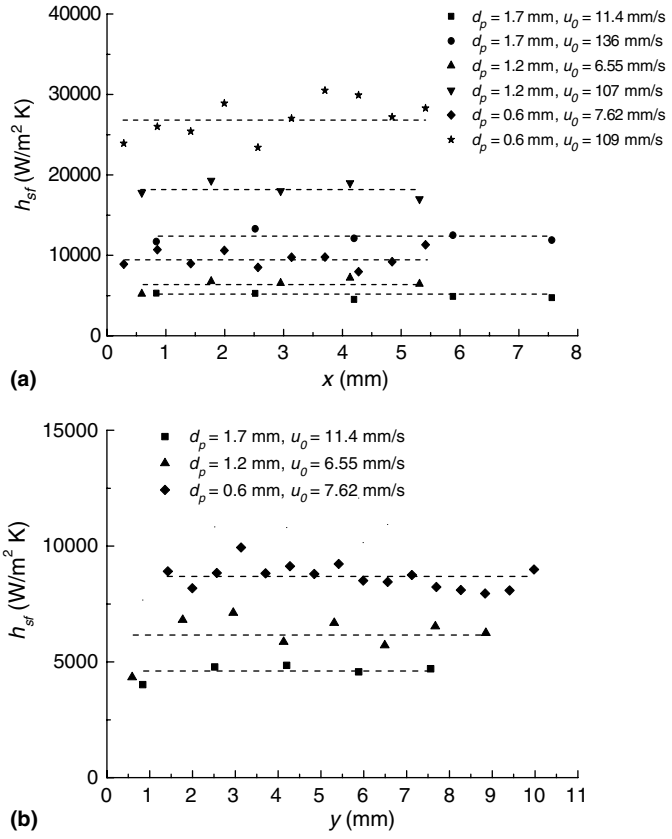

Fig. 8. Variation of the heat transfer coefficients between the solid particles and the fluid (a) in the flow direction for the second row of particles, (b) in the vertical direction for the third column of particles.

Fig. 8(b) shows the heat transfer coefficients between the fluid and the solid particles for the third column of particles from the inlet in porous media with various particle diameters and fluid velocities. The heat transfer coefficients decrease with particle diameter and do not change much in the y-direction.

Fig. 9 compares the calculated heat transfer coefficients between the solid particles and the fluid with predicted values from Eqs. (17) and (18) for the three particle diameters. The numerically predicted heat transfer coefficients correspond reasonably well with the predictions of Eqs. (17) and (18) for all three diameters. The deviations between the calculated and empirical results were mostly less than 30%. The differences between the models are due to the differences between the ideal porous media in the numerical model and real porous media. Both models indicate that the heat transfer coefficients increase with particle Reynolds number and decrease with increasing particle diameter. The volumetric heat transfer coefficient, h_v, was then calculated using Eq. (21).

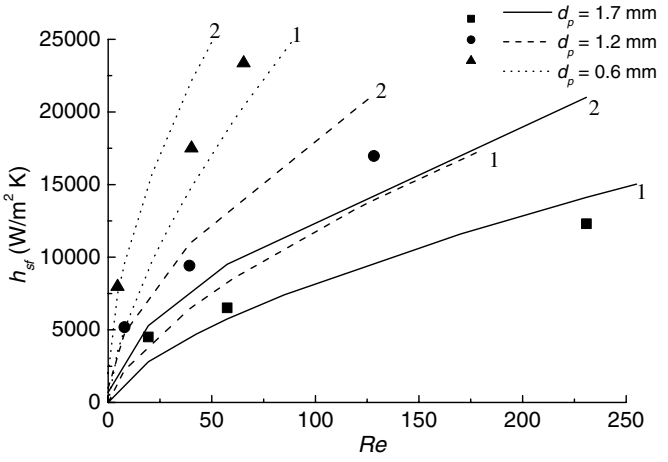

Fig. 9. Comparison of the predicted heat transfer coefficients between the solid particles and the fluid from the numerical solution and from Eq. (17) (line 1) and Eq. (18) (line 2).

3.5. Temperature distributions and local thermal non-equilibrium in porous media

Fig. 10 shows the average temperature distribution in the solid particles in the third column from the inlet and in the fluid along the y-direction. The thermal non-equilibrium

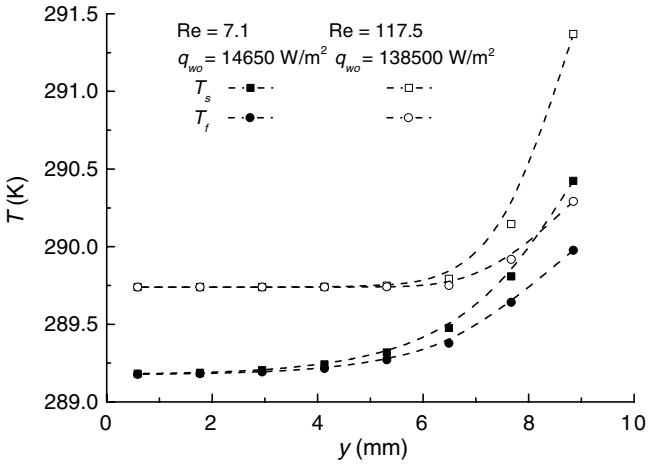

Fig. 10. Average temperature variations in the solid particles in the third column and in the fluid in the vertical direction for $d_p = 1.2$ mm and $\varepsilon_m = 0.450$. (■, ●)—$u_0 = 6.55$ mm/s, $T_{f0} = 289.17$ K, $q_{w0} = 14{,}650$ W/m^2; (□, ○)—$u_0 = 107$ mm/s, $T_{f0} = 289.74$ K, $q_{w0} = 138{,}500$ W/m^2.

shown by the temperature difference between the solid particles and the fluid is evident. The differences between the average particle and fluid temperatures reaches a maximum in the first row of particles and then decreases further from the heated surface. The temperature differences increase with increasing heat flux. The thermal penetration thickness also decreases with increasing velocity. Therefore, numerical simulations of convection heat transfer in porous media should use a thermal non-equilibrium model.

4. Conclusions

Flow and convection heat transfer of water in a sintered bronze porous channel was investigated numerically in this work. The complicated structure of the porous channel was fully simulated to match the experimental setup.

(1) The numerical results for the permeability, K, and the inertia coefficient, F, defined by the modified Darcy's model agree well with theoretical predictions.
(2) The local heat transfer coefficients predicted by the numerical model agreed well with experimental data. The local heat transfer coefficients increased with mass flow rate and decreased slightly along the axial direction. The numerical results also illustrate the temperature difference between the solid particles and the fluid which indicates the importance of using the thermal non-equilibrium model when analyzing flow in porous media.
(3) The numerically predicted heat transfer coefficients between the solid particles and the fluid agree well with the predictions of Eqs. (17) and (18), with increases as the particle Reynolds number increases and decreases with increasing particle diameter.
(4) The temperature fields in the solid particles and the fluid show that the thermal penetration and thermal boundary layer thicknesses increase along the flow direction and decrease with increasing velocity.

Acknowledgements

The project was supported by the National Outstanding Youth Fund from the National Natural Science Foundation of China (No. 50025617). We also thank Dr. David Christopher for editing the English.

References

[1] K. Vafai, C.L. Tien, Boundary and inertial effects on flow and heat transfer in porous media, Int. J. Heat Mass Transfer 24 (1981) 195–203.
[2] C.T. Hsu, P. Cheng, Thermal dispersion in a porous medium, Int. J. Heat Mass Transfer 33 (8) (1990) 1587–1597.
[3] C.Y. Choi, F.A. Kulacki, Non-Darcian effects on mixed convection in a vertical porous annulus, in: Proc. 9th IHTC-Heat Transfer, vol. 5, 1990, pp. 271–276.
[4] E. David, G. Lauriat, P. Cheng, A numerical solution of variable porosity effects on natural convection in a packed-sphere cavity, J. Heat Transfer 113 (1991) 391–399.
[5] N.J. Kwendakwema, R.F. Boehm, Parametric study of mixed convection in a porous medium between vertical concentric cylinders, J. Heat Transfer 113 (1991) 128–134.
[6] P.X. Jiang, B.X. Wang, D.A. Luo, Z.P. Ren, Fluid flow and convective heat transfer in a vertical porous annulus, Numer. Heat Transfer A 30 (3) (1996) 305–320.
[7] P.X. Jiang, Z.P. Ren, B.X. Wang, Numerical simulation of forced convection heat transfer in porous plate channels using thermal equilibrium or non-thermal equilibrium models, Numer. Heat Transfer A 35 (1) (1999) 99–113.
[8] E. Achenbach, Heat and flow characteristics of packed beds, Exp. Therm. Fluid Sci. 10 (1) (1995) 17–27.
[9] A. Amiri, K. Vafai, Analysis of dispersion effects and non-thermal equilibrium, non-Darcian, variable porosity incompressible flow through porous media, Int. J. Heat Mass Transfer 37 (6) (1994) 939–954.
[10] W.H. Hsieh, S.F. Lu, Heat-transfer analysis and thermal dispersion in thermally-developing region of a sintered porous metal channel, Int. J. Heat Mass Transfer 43 (16) (2000) 3001–3011.
[11] B. Alazmi, K. Vafai, Constant wall heat flux boundary conditions in porous media under local thermal non-equilibrium conditions, Int. J. Heat Mass Transfer 45 (15) (2002) 3071–3087.
[12] A. Amiri, K. Vafai, T.M. Kuzay, Effects of boundary conditions on non-Darcian heat transfer through porous media and experimental comparisons, Numer. Heat Transfer A 27 (6) (1995) 651–664.
[13] M. Quintard, Modelling local non-equilibrium heat transfer in porous media, in: Proc. of 11th Int. Heat Transfer Conference on Heat Transfer 1998, Kyongju, Korea, vol. 1, 1998, pp. 279–285.
[14] G.P. Peterson, C.S. Chang, Two-phase heat dissipation utilizing porous-channels of high-conductivity materials, J. Heat Transfer 120 (1) (1998) 243–252.
[15] A.R. Martin, C. Saltiel, W. Shyy, Heat transfer enhancement with porous inserts in recirculating flows, J. Heat Transfer 120 (2) (1998) 458–467.
[16] D.Y. Lee, K. Vafai, Analytical characterization and conceptual assessment of solid and fluid temperature differences in porous media, Int. J. Heat Mass Transfer 42 (3) (1999) 423–435.
[17] P.X. Jiang, Z.P. Ren, Numerical investigation of forced convection heat transfer in porous media using a thermal non-equilibrium model, Int. J. Heat Fluid Flow 22 (1) (2001) 102–110.

[18] P.X. Jiang, M. Li, Z.P. Ren, Forced convection heat transfer in plate channels filled with packed beds or sintered porous media, Tsing. Sci. Technol. 7 (2) (2002) 202–208.
[19] P.X. Jiang, M. Li, Y.C. Ma, Z.P. Ren, Boundary conditions and wall effect for forced convection heat transfer in sintered porous plate channels, Int. J. Heat Mass Transfer 47 (10–11) (2004) 2073–2083.
[20] M. Golombok, H. Jariwala, L.C. Shirvill, Gas–solid heat exchange in a fibrous metallic material measured by a heat regenerator technique, Int. J. Heat Mass Transfer 33 (1990) 243–252.
[21] K. Vafai, M. Sozen, Analysis of energy and momentum transport for fluid flow through a porous bed, J. Heat Transfer 112 (1990) 690–699.
[22] B.W. Gamson, G. Thodos, O.A. Hougen, Heat, mass and momentum transfer in the flow of gases through granular solids, AIChE J. 39 (1943) 1–35.
[23] K. Ichimiya, A new method for evaluation of heat transfer between solid material and fluid in a porous medium, J. Heat Transfer 121 (4) (1999) 978–983.
[24] P.X. Jiang, M. Li, T.J. Lu, L. Yu, Z.P. Ren, Experimental research on convection heat transfer in sintered porous plate channels, Int. J. Heat Mass Transfer 47 (10–11) (2004) 2085–2096.
[25] FLUENT User's Guide, Release 6.1. FLUENT Inc., Lebanon, 2001.
[26] P. Zehener, Waermeleitfahigkeit won Schuettungen be Massigen Temperaturea, Chem.-Ingr.-Tech. 42 (1970) 933–941.
[27] P. Forchheimer, Wasserbewegung durch Boden, Z. Verein Deutscher Ing. 45 (1901) 1782–1788.
[28] M. Kaviany, Principles of Heat Transfer in Porous Media, Springer-Verlag, New York, 1991.
[29] A.G. Dixon, D.L. Cresswell, Theoretical prediction of effective heat transfer parameters in packed beds, AIChE J. 25 (4) (1979) 663–676.
[30] N. Wakao, S. Kaguei, Heat and Mass Transfer in Packed Beds, Gordon and Breach, New York, 1982.
[31] F.P. Incropera, D.P. DeWitt, Fundamentals of Heat and Mass Transfer, fourth ed., John Wiley & Sons, 1996.